

# Transition Metal Induced Crystallization of Ultrathin Silica Films

Linfei Li, Heloise Tissot, Shamil Shaikhutdinov,\*<sup>1b</sup> and Hans-Joachim Freund<sup>1b</sup>

Department of Chemical Physics, Fritz Haber Institute of the Max Planck Society, Faradayweg 4-6, 14195 Berlin, Germany

Silica (SiO<sub>2</sub>) is one of the key materials in many modern technological applications including microelectronics, catalysis, and photonics.<sup>1–4</sup> As an ultrathin film grown on metal surfaces,<sup>5–7</sup> silica becomes an attracting material for a new generation of the metal oxide–semiconductor transistors and further miniaturization of electronic devices.<sup>8</sup> The structural motif of such films is a hexagonal layer of corner sharing SiO<sub>4</sub> tetrahedra, i.e., a single silicate layer or the so-called “silicatene”,<sup>9</sup> which nicely fits a growing family of truly two-dimensional (2D) materials such as graphene, silicene, etc. Although technologically relevant properties of ultrathin silicate films, so far addressed by theory (see, for instance, ref 10), remain to be thoroughly explored in experiments, the controllable preparation of the well-defined, crystalline films is crucial for establishing and understanding of their structure–property relationships, which can, in turn, provide a basis for their potential application.

In the great majority of cases, single-layer silicate films are obtained in the crystalline form, most likely due to the strong interaction with the metal single crystal surface via Si–O–metal linkages, whereas a silicate bilayer terminated by oxygen on either side is weakly bound to the metal surface and primarily exists in the laterally amorphous state. The latter is now recognized as a 2D analogue of silica glass,<sup>11–14</sup> which allows glass transitions to be studied at the atomic level.<sup>15</sup> Figure 1a

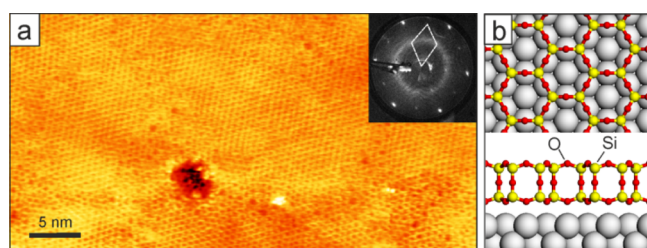


**Figure 1.** (a) STM image of a bilayer silicate film prepared at 1250 K which exposes both the crystalline and the amorphous domains. The corresponding LEED pattern (in the inset) shows the Ru(0001)–(2 × 2) diffraction spots, arising from the crystalline honeycomb-like structure schematically shown in panel (b), as well as the diffraction ring reflecting the disordered phase. A small depression in the central portion of the STM image exposes a single layer silicate. Tunneling parameters are bias 1.2 V, current 0.22 nA.

displays a high-resolution scanning tunneling (STM) image of a well-ordered bilayer silicate film grown on Ru(0001), with both crystalline and amorphous phases coexisting, as judged by the low energy electron diffraction (LEED) pattern showing both the diffraction spots and the diffraction ring, which is characteristic for randomly oriented domains. The atomic structure of a crystalline bilayer silicate film is schematically shown in Figure 1b.

Further studies on silicate films modified by other metals (Al, Fe, Ti) revealed certain structural effects of the metal used. Al substitutes Si in the framework such that the bilayer structure is maintained, although the replacement starts within the bottom silicate layer and apparently follows the so-called Löwenstein rule (the principle of Al–O–Al avoidance).<sup>16,17</sup> In contrast, Fe- and Ti-containing films showed Fe(Ti) segregation within the bottom layer thus forming the FeO<sub>x</sub>(111)- (respectively, TiO<sub>x</sub>(111)-like) layer underneath the silicate layer (Figure 2d).<sup>18,19</sup> Such a two-layer structure, hereafter referred to as

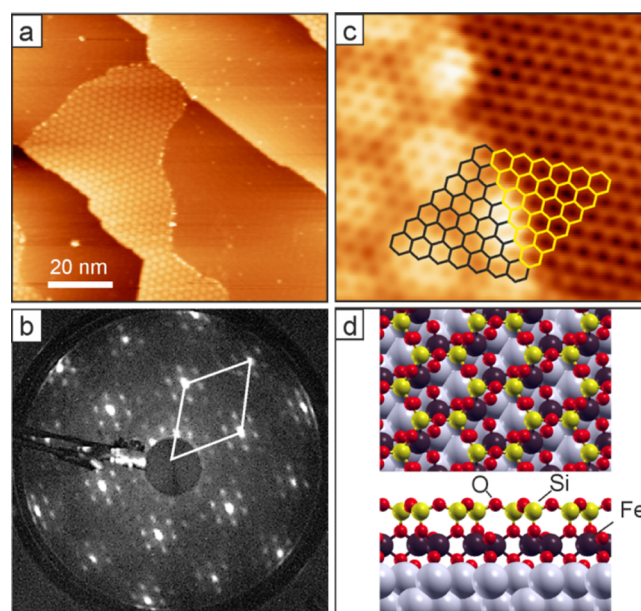


**Figure 2.** (a) Large-scale STM image of an Fe-containing film prepared at 1100 K showing phase separation into Fe–silicate (visible via strong Moiré structure) and surrounded pure bilayer silicate. The corresponding LEED pattern (at 70 eV) is shown in panel (b). The unit cell of the “30°-rotated” structure is indicated. (c) High-resolution STM image of the interface between two phases superimposed with the polygonal silicate network. (Tunneling parameters are 1.3 V and 0.12 nA (a); 1.5 V and 0.16 nA (b)). (d) Structural model of the Fe–silicate in top and cross views.

Fe(Ti)–silicate, bears close similarities to the principal structure of clay minerals. In addition, the films at low Fe(Ti):Si ratios showed phase separation, i.e., Fe(Ti)–silicate and pure bilayer silicate form individual phases (Figure 2a). Importantly, all previously studied (Al, Fe, Ti) substituted films as well as recently studied Fe-modified aluminosilicate films<sup>20</sup>

Received: December 9, 2016

Revised: January 19, 2017

Published: January 27, 2017

showed almost 100% crystallinity, even though being prepared at considerably lower annealing temperatures than those used for pure silicate films.

LEED and STM studies showed that the Al–silicate films exhibit a  $(2 \times 2)$  periodicity with respect to the Ru(0001) surface, thus resulting in the surface lattice constant of 5.42 Å, i.e., the same as for crystalline pure silicate films. In the case of the Fe-substituted films, however, the entire film (i.e., both Fe–silicate and pure silicate domains) is rotated by  $30^\circ$  and exhibits a 5.22 Å lattice constant, i.e., considerably shorter than in pure silicate. On the basis of the density functional theory (DFT) calculations performed so far for a  $(2 \times 2)$  periodic slab,<sup>18</sup> Fe–silicate is more strongly bound to the Ru(0001) surface. In principle, this may explain the enhanced long-range ordering (“crystallization”) due to the formation of the Fe–O–Ru linkages at the interface leading to a stronger adhesion to the Ru(0001) surface (see model in Figure 2d). However, this finding standing alone can hardly explain the  $30^\circ$  rotation resulting in a Moiré-like coincidence structure incommensurate with respect to the Ru(0001) surface. Apparently, DFT calculations on the large Moiré supercell must be performed to shed more light on this issue. Note that a pure monolayer FeO(111) film is not rotated with respect to Ru(0001) (and Pt(111)),<sup>21</sup> even though it forms a Moiré pattern.

Another factor that often affects thin film epitaxial growth is the lattice mismatch between the film and the substrate. On the basis of the DFT calculations, an unsupported free-standing silicate bilayer would show a lattice constant of about 5.30 Å.<sup>7,22,23</sup> This implies a certain in-plane distortion (stretch or stress) either to fit 5.42 Å, observed on Al–silicate films showing a  $(2 \times 2)$ -Ru(0001) LEED pattern, or 5.22 Å, observed on the Fe–silicate films rotated by  $30^\circ$  with respect to Ru(0001) (which are, for brevity, henceforth referred to as “ $(2 \times 2)$ ” and “ $30^\circ$ -rotated” structures, respectively). In principle, interaction with a metal surface and how well the silicate lattice matches the metal surface both may affect crystallinity and orientation of the resulted films. However, the question remains: why is the bilayer silicate in the Fe-free surface regions also rotated, whereas it forms a nonrotated  $(2 \times 2)$  structure in the pure silicate films? Indeed, Figure 2b nicely shows that the silicate layer follows the same registry upon crossing the border from the Fe–silicate to the pure silicate region. (The Fe–silicate domain appears higher, most likely due to electronic effects in STM.) Another intriguing question is the following: why in all metal-modified films is the pure silicate phase crystalline even at low metal concentrations?

In attempts to answer these questions, we recall that growth of 3D-crystals typically follows an initial stage of nucleation, i.e., the formation of a small nucleus containing the newly forming crystallites. After the nucleation, the crystal homoepitaxially grows outward from the nucleating site. As the nucleation process is relatively slow in a homogeneous systems, a “seed” crystallite is commonly added to accelerate this. In principle, one could envision that similar processes occur in 2D-systems, such as ultrathin films considered here. To investigate the role of Fe in the nucleation-and-growth process, in this work we monitored the Fe–silicate film formation by LEED, STM, and infrared reflection–absorption spectroscopy (IRAS).

Figure 3a displays a LEED pattern of the sample prepared by brief annealing at 1050 K. It clearly exhibits the “ $30^\circ$ -rotated” structure as for the well-annealed Fe–silicate films (Figure 2b). However, there are additional relatively strong  $(2 \times 2)$  spots and, more interestingly, a faint diffraction ring, which are

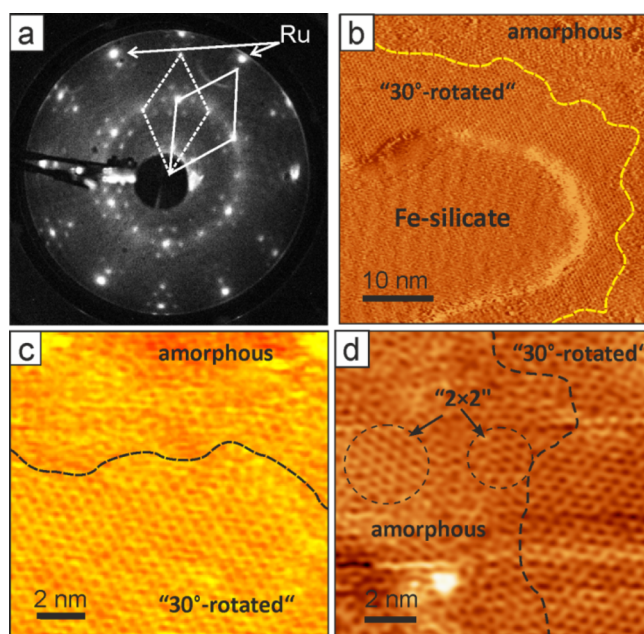


**Figure 3.** (a) LEED pattern (at 70 eV) of the Fe-containing silicate film prepared at 1050 K. The unit cells of the “ $30^\circ$ -rotated” and “ $(2 \times 2)$ ” structures are indicated by solid and dashed rhombuses, respectively. In addition, a faint diffraction ring, which is virtually identical to that shown in Figure 1a, is observed. (b) STM image of this sample presented in the differentiated contrast. An Fe–silicate domain is surrounded by a “ $30^\circ$ -rotated” crystalline silicate layer as zoomed in panel (c). The dashed curves guide the eye to separate crystalline and amorphous portions. Image (d) shows also small  $(2 \times 2)$  domains observed within the amorphous regions. Tunneling bias and currents are 1.2 V and 0.25 nA for all images.

characteristic for the amorphous pure silicate film (inset in Figure 1a). In full agreement with the LEED results, the STM images showed islands of Fe–silicate exposing a Moiré structure. However, a close STM inspection revealed the “ $30^\circ$ -rotated” pure silicate structure only in regions surrounding and/or in direct contact to the Fe–silicate domains (Figure 3b). Farther away, the film is amorphous and shows the atomic structure of pure silicate films usually formed in the absence of Fe, where small  $(2 \times 2)$  domains are “dissolved” in amorphous regions (Figures 3c,d).

Figure 4 collects the IRA spectra recorded on the Fe–silicate sample after stepwise oxidation treatment at increasing temperature as indicated. To recall, the IRAS bands at 1300 and 692  $\text{cm}^{-1}$  belong to the pure silicate bilayer structure regardless of the film crystallinity.<sup>24</sup> The band at 1002  $\text{cm}^{-1}$  is a fingerprint of the Fe–silicate structure reflecting the formation of Si–O–Fe bonds.<sup>18</sup> Finally, the asymmetric broad band centered at 1252  $\text{cm}^{-1}$  is commonly associated with amorphous silica films, e.g., thermally grown on Si surfaces.<sup>25,26</sup> Following this assignment, it is clear that the Fe–silicate phase forms at relatively low temperatures (1000 K), at which pure silica phase primarily exists as amorphous, 3D silica structures, most likely in a nanoparticulate form.<sup>20,27</sup> At increasing temperature to 1050 K, a bilayer silicate film starts to form, as the two bands at 1300 and 692  $\text{cm}^{-1}$  show up simultaneously with the 1252  $\text{cm}^{-1}$  band disappearing. In line with the LEED results, the film becomes better ordered upon further oxidation treatment as both the pure silicate and the Fe–silicate related bands gain intensity. However, further increasing temperatures up to 1200

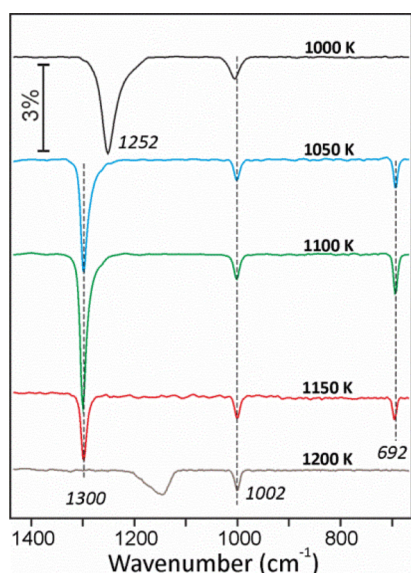


**Figure 4.** IR spectra of the Fe-silicate film as a function of oxidation temperature as indicated. For the band assignment, please refer to the text.

K leads to the film decomposition (sublimation and/or dewetting), although the Fe-silicate phase remains, i.e., in line with its stronger interaction with the metal surface via Fe-O-Ru bonds at the interface. It is important to note that, in the absence of Fe, the formation of bilayer silicate film starts at a considerably higher temperature ( $\sim 1200$  K), as judged by IRAS. However, the pure silicate film remains stable even at 1275 K.

Therefore, on the basis of above-presented LEED, STM, and IRAS results, we propose that the Fe-silicate phase upon formation at relatively low temperatures triggers the formation of the crystalline bilayer silicate structure which propagates as a “crystallization wave” outward the Fe-silicate. It is the  $30^\circ$ -rotated Fe-silicate domain, formed at the early stage due to the strong interaction with the metal surface, that drives the silicate bilayer film to grow in the same orientation. This scenario is schematically illustrated in Figure 5. Therefore, one may refer to Fe (and possibly other transition metals) as a “crystal former” in analogy to the “glass formers” used for the glassy systems.

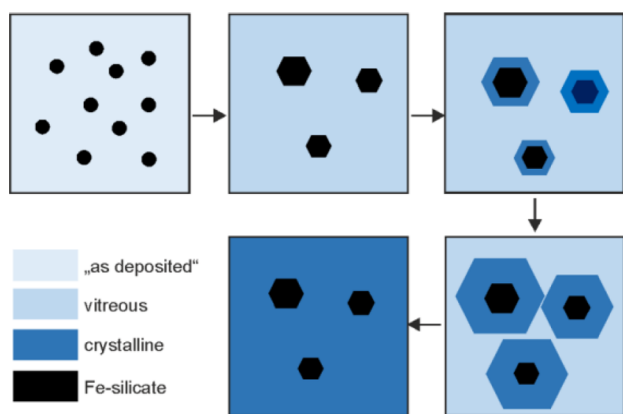


**Figure 5.** Proposed scenario for the growth of the crystalline Fe-modified films.

As previously shown by DFT,<sup>18</sup> the formation of the Fe-silicate structure with a silicate layer on top of an FeO(111)-like layer is energetically much more favorable as compared to the Fe substitution of the Si atoms in the bilayer silicate framework. This may explain the early formation of the Fe-silicate domains at relatively low temperatures. Once formed, these domains behave as a “seed” to crystallize the remaining silica in the form of bilayer silicate through a good epitaxial relationship at the interface to the Fe-silicate (Figure 2c). The crystallization process likely propagates until a crystalline silicate bilayer covers the entire substrate not occupied by Fe-silicate. The formation temperature of a crystalline silicate layer in the Fe-containing films is considerably lower than in the pristine silicate films, which are mostly dominated by the amorphous phase even at considerably higher temperatures. Therefore, using transition metal as “a seed” one may substantially improve film crystallinity and lower the preparation temperature, which may be important for technological applications based on the ultrathin silica films yet remain to be explored.

The experiments were carried out in an UHV chamber equipped with STM (Omicron), LEED (Omicron), XPS with Scienta SES 200 analyzer, and IRAS (Bruker IFS 66v). The Ru(0001) crystal (MaTeck GmbH) was mounted on an Omicron sample holder, and the temperature was measured by a Type K thermocouple spot-welded to the edge of the crystal. The Ru(0001) crystal was cleaned by several cycles of Ar<sup>+</sup> ion sputtering and annealing at 1400 K and checked by XPS, LEED, and STM prior to the film growth. The clean Ru(0001) surface was precovered with a 3O-(2 × 2) adlayer by exposing to  $3 \times 10^{-6}$  mbar O<sub>2</sub> at 1200 K for 5 min and cooling to 500 K before oxygen was pumped out. Then Si was evaporated from the e-beam assisted evaporator (EMT3, Omicron) at 100 K in  $2 \times 10^{-7}$  mbar O<sub>2</sub>. The samples were oxidized at 1200–1250 K in  $3 \times 10^{-6}$  mbar O<sub>2</sub> for 10 min and slowly cooled down to 500 K before oxygen was pumped out. Fe-containing silicate films were prepared by sequential Si and Fe deposition at 100 K in  $2 \times 10^{-7}$  mbar O<sub>2</sub> at total amounts equivalent to form a silicate bilayer framework as measured by XPS. The films were oxidized in  $3 \times 10^{-6}$  mbar O<sub>2</sub>. The IRAS-spectra were recorded using p-polarized light at  $84^\circ$  grazing angle of incidence (resolution 4 cm<sup>-1</sup>). The STM images were obtained at room temperature using W tips.

## ■ AUTHOR INFORMATION

### Corresponding Author

\*(S.S.) E-mail: [shaikhutdinov@fhi-berlin.mpg.de](mailto:shaikhutdinov@fhi-berlin.mpg.de).

### ORCID

Shamil Shaikhutdinov: 0000-0001-9612-9949

Hans-Joachim Freund: 0000-0001-5188-852X

### Author Contributions

The manuscript was written through contributions of all authors.

### Funding

The work was supported by Deutsche Forschungsgemeinschaft through SFB 1109 and Fonds der Chemischen Industrie.

### Notes

The authors declare no competing financial interest.

## ■ REFERENCES

(1) Hattori, T.; et al. Chemical and Electronic Structure of SiO<sub>2</sub>/Si Interfacial Transition Layer. *Appl. Surf. Sci.* **2003**, *212–213*, 547–555.

- (2) Helms, C. R.; Poindexter, E. H. The Silicon-Silicon Dioxide System: Its Microstructure and Imperfections. *Rep. Prog. Phys.* **1994**, *57*, 791.
- (3) Legrand, A. P., ed. *The Surface Properties of Silicas*; John Wiley and Sons Ltd: New York, 1998; p 465.
- (4) Zhuravlev, L. T. The Surface Chemistry of Amorphous Silica. Zhuravlev Model. *Colloids Surf, A* **2000**, *173*, 1–38.
- (5) Shaikhutdinov, S.; Freund, H.-J. Ultrathin Silica Films on Metals: The Long and Winding Road to Understanding the Atomic Structure. *Adv. Mater.* **2013**, *25*, 49–67.
- (6) Shaikhutdinov, S.; Freund, H.-J. Ultra-thin Silicate Films on Metals. *J. Phys.: Condens. Matter* **2015**, *27*, 443001.
- (7) Altman, E. I.; et al. Growth and Characterization of Crystalline Silica Films on Pd(100). *J. Phys. Chem. C* **2013**, *117*, 26144–26155.
- (8) Muller, D. A.; et al. The Electronic Structure at the Atomic Scale of Ultrathin Gate Oxides. *Nature* **1999**, *399*, 758–761.
- (9) Yang, B.; et al. Patterned Defect Structures Predicted for Graphene are Observed on Single-Layer Silica Films. *Nano Lett.* **2013**, *13*, 4422–4427.
- (10) Han, Y.; et al. Strain-modulated Electronic and Thermal Transport Properties of Two-dimensional O-silica. *Nanotechnology* **2016**, *27*, 265706.
- (11) Heyde, M.; Shaikhutdinov, S.; Freund, H. J. Two-dimensional silica: Crystalline and Vitreous. *Chem. Phys. Lett.* **2012**, *550*, 1–7.
- (12) Lichtenstein, L.; et al. The Atomic Structure of a Metal-Supported Vitreous Thin Silica Film. *Angew. Chem. Int. Ed.* **2012**, *51*, 404–407.
- (13) Büchner, C.; et al. Ultrathin Silica Films: The Atomic Structure of Two-Dimensional Crystals and Glasses. *Chem. - Eur. J.* **2014**, *20*, 9176–9183.
- (14) Huang, P. Y.; et al. Direct Imaging of a Two-Dimensional Silica Glass on Graphene. *Nano Lett.* **2012**, *12*, 1081–1086.
- (15) Huang, P. Y.; et al. Imaging Atomic Rearrangements in Two-Dimensional Silica Glass: Watching Silica's Dance. *Science* **2013**, *342*, 224–227.
- (16) Boscoboinik, J. A.; et al. Modeling Zeolites with Metal-Supported Two-Dimensional Aluminosilicate Films. *Angew. Chem., Int. Ed.* **2012**, *51*, 6005–6008.
- (17) Shaikhutdinov, S.; Freund, H.-J. Metal-Supported Aluminosilicate Ultrathin Films as a Versatile Tool for Studying the Surface Chemistry of Zeolites. *ChemPhysChem* **2013**, *14*, 71–77.
- (18) Włodarczyk, R.; et al. Atomic Structure of an Ultrathin Fe-Silicate Film Grown on a Metal: A Monolayer of Clay? *J. Am. Chem. Soc.* **2013**, *135*, 19222–19228.
- (19) Fischer, F. D.; et al. Ultrathin Ti-Silicate Film on a Ru(0001) Surface. *J. Phys. Chem. C* **2015**, *119*, 15443–15448.
- (20) Tissot, H.; et al. Preparation and Structure of Fe-containing Aluminosilicate Thin Films. *Phys. Chem. Chem. Phys.* **2016**, *18*, 25027–25035.
- (21) Ketteler, G.; Ranke, W. Heteroepitaxial Growth and Nucleation of Iron Oxide Films on Ru(0001). *J. Phys. Chem. B* **2003**, *107*, 4320–4333.
- (22) Gao, E.; Xie, B.; Xu, Z. Two-dimensional Silica: Structural, Mechanical Properties, and Strain-induced Band Gap Tuning. *J. Appl. Phys.* **2016**, *119*, 014301.
- (23) Han, Y.; Hu, M. Ground State of Bilayer h  $\alpha$  -Silica: Mechanical and Electronic Properties. *Nanotechnology* **2015**, *26*, 505702.
- (24) Löffler, D.; et al. Growth and Structure of Crystalline Silica Sheet on Ru(0001). *Phys. Rev. Lett.* **2010**, *105*, 146104.
- (25) Stacchiola, D. J.; et al. Growth of Stoichiometric Subnanometer Silica Films. *Appl. Phys. Lett.* **2008**, *92*, 011911–3.
- (26) Queeney, K. T.; et al. Infrared Spectroscopic Analysis of the Si/SiO<sub>2</sub> Interface Structure of Thermally Oxidized Silicon. *J. Appl. Phys.* **2000**, *87*, 1322–1330.
- (27) Kaya, S.; et al. On the Geometrical and Electronic Structure of an Ultra-thin Crystalline Silica Film Grown on Mo(112). *Surf. Sci.* **2007**, *601*, 4849–4861.